

Phononic properties of cinnabar: Ab initio calculations and new experimental results

R.K. Kremer, M. Cardona, R. Lauck, G. Siegle, A. Muñoz¹, A.H. Romero² and M. Schmidt³

Cinnabar (α -HgS) is the main ore for the production of mercury and, in powdered form, constitutes the red pigment *vermillion* which was already used in pre-Columbian Peru as early as 500 BC (Chavin Empire). Large scale mining of cinnabar is known to have taken place after the conquest of the Inca Empire (1532 AD) in connection with the extraction of silver from low grade ores. It probably led to the first pre-industrial source of Hg environmental pollution. Evidence for the use of cinnabar as a pigment is also found in Mesoamerica, dating back to the Olmec culture (\approx 800 BC), where it was utilized in ceremonial burials and for coloring beautiful ceramic figurines.

In the Eastern World, China, today the main producer of mercury, was early using cinnabar as a pigment. The best known use is found in the lacquerware of the Song Dynasty (1000 AD). Cinnabar is applied, still today, in traditional Chinese medicine (as *Zhu Sha*) to treat a variety of ailments including colds, insomnia, restlessness and, less dangerously since applied externally, skin disorders. Because of the existence of large cinnabar deposits, *vermillion* was also used in Spain and Italy to illuminate ancient manuscripts.

The extraction of mercury from cinnabar is already documented in Teophrastus of Eresus' 'Book on Stones' (\approx 315 BC): 'Native cinnabar was rubbed with vinegar in a copper mortar with a copper pestle', thus describing what is probably the first mechano-chemical reaction. Pliny the Elder (23-79 AD), in his natural history [1], describes not only the mechano-chemical but also the distillation method which seems to have originated from Dioscorides (40-90 AD).

Cinnabar is the stable form of HgS under normal temperature and pressure. Besides, a zincblende-type modification of HgS, metacinnabar

(β -HgS), also exists. We have described its electronic and vibronic properties in the Annual Report of 2009.

Despite the wide technological importance of cinnabar there is limited knowledge of its electronic and lattice dynamical properties. In this contribution we focus on the phonon and thermodynamic properties of cinnabar. Especially, we calculate the phonon dispersion relations and compare theoretical results with our new experimental data and data available in the literature. The reader may find a more detailed discussion of the electronic structure and derived optical properties of cinnabar including a comparison of the calculated dielectric function with unpublished experimental data in [2].

Cinnabar has two chiral (enantiomorphic) structure modifications (space groups no. 152 (D_3^4) and no. 154 (D_3^6), the primitive cell is composed of two coaxial helices, one with three S atoms, the other with three Hg atoms). These modifications rotate the plane of polarization of light propagating along the c -axis in opposite directions (optical activity).

The *ab initio* calculations have been performed with two different implementations of Density Functional Theory, the VASP and the ABINIT code [2]. The latter was used to obtain the vibrational properties. To this end the dynamical matrices were calculated for a grid of $6 \times 6 \times 3$ and four different grid shifts, with a total of 83 matrices (including the Γ point) and a Fourier interpolation was carried out in order to increase the density of \mathbf{q} points.

We display in Fig. 1 the phonon dispersion relations of cinnabar. The 6 atoms per primitive cell give rise to 18 vibrational modes, 3 of which have zero frequency at Γ (acoustic modes). Thus we are left with 15 modes, $5\Gamma_3$ doublets (ir and Raman active), $2\Gamma_1$ singlets (Raman active) and $3\Gamma_2$ singlets (ir active). The

ir active modes split into longitudinal and transverse, depending on whether the E -field is parallel or perpendicular to the scattering vector, the splitting being determined by Born effective charges. It is worth noticing that the five Γ_3 doublets ($\approx 43 \text{ cm}^{-1}$, $\approx 85 \text{ cm}^{-1}$, $\approx 122 \text{ cm}^{-1}$, $\approx 263 \text{ cm}^{-1}$ and $\approx 321 \text{ cm}^{-1}$) split linearly in \mathbf{k} along the Γ -A direction. This splitting is induced by the chirality of the structure and should be responsible for optical activity related to the ir-active phonons.

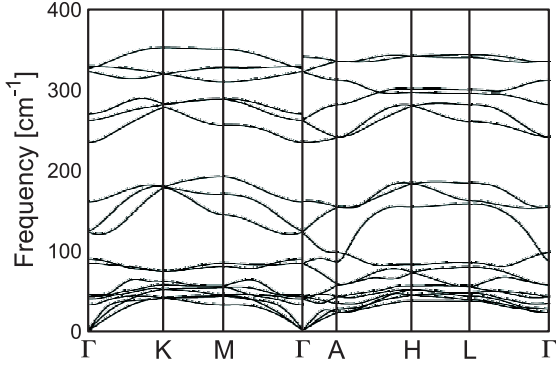


Figure 1: Calculated phonon dispersion of α -HgS. The calculations have been performed without taking spin-orbit coupling into account. Calculations carried out by taking spin-orbit coupling into account revealed changes of the Γ -point phonon energies compared to these results of less than $\approx 1.5\%$.

Regrettably there are no experimental data available for the phonon dispersion relations throughout the whole Brillouin zone. The only experimental phonon data published are those obtained with Raman and ir spectroscopy at the zone center [3]. These agree reasonably well with our calculations, especially if one considers the complexity of the crystal structure of α -HgS, with six atoms per unit cell.

Figure 2 shows the phonon density of states (PDOS) calculated from the dispersion relations and its decomposition into S-like and Hg-like partial components. As expected, the low-frequency band ($0-100 \text{ cm}^{-1}$) corresponds mainly to Hg vibrations whereas that between 230 cm^{-1} and 350 cm^{-1} is mainly sulfur-like. It is interesting to notice that the intermediate band, between 110 cm^{-1} and 190 cm^{-1} , is almost pure sulfur-like.

The PDOS displayed in Fig. 1 was used to calculate the total energy, $F(T)$, and the specific heat at constant volume, $C_v(T)$, by taking the

second derivative of the total energy. In order to compare with experimental data we have extended available low-temperature heat capacity measurements up to $\approx 350 \text{ K}$ on several samples comprising natural and artificial crystals of α -HgS including such with isotope enrichment either for Hg or S. These have been grown by conventional vapor phase transport techniques [4].

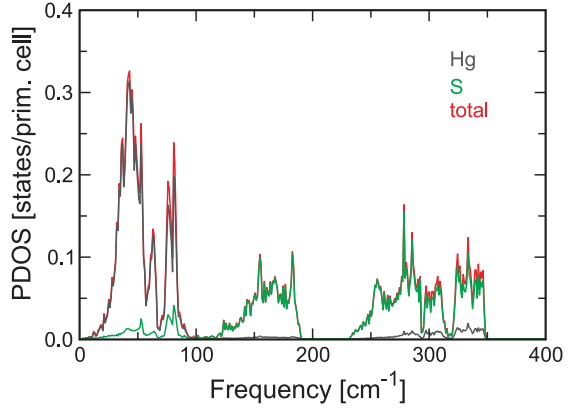


Figure 2: Phonon density of states (PDOS); partial contributions from Hg and S and the total PDOS are displayed.

To emphasize the low-temperature regime and to follow deviations from Debye's T^3 -power law our experimental data are shown in a C_p/T^3 plot. Figure 3 illustrates the very good agreement of our experimental data with those of Khattak *et al.* and the agreement of the data obtained on natural or artificial α -HgS crystals. The C_p/T^3 -plot reveals the characteristic maximum at $\approx 10 \text{ K}$ which had actually been observed at 7 K for the zincblende modification (β -HgS). The position of this maximum is usually determined by the lowest maximum of the PDOS which, according to Fig. 2 appears at 65 K . The ratio $65/10=6.5$ is typical for the maximum of C_p/T^3 in many semiconductors. Near the maximum in C_p/T^3 the theory points fall short by about 3.5% . Above 20 K , up to 250 K there is good agreement of experimental and theoretical results. Above 250 K the theoretical data approach the Petit-Dulong limit of $6 \times R$, where R is the molar gas constant, somewhat slower than the experimental data. Almost perfect agreement is achieved when thermal expansion effects are taken into account [2].

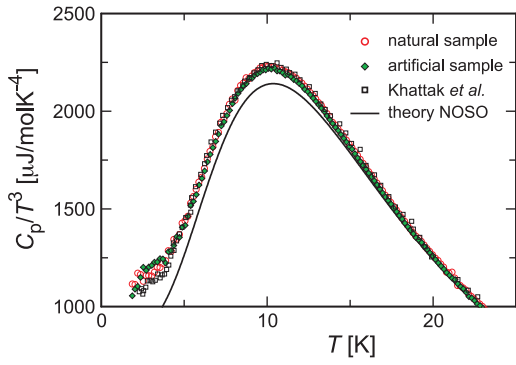


Figure 3: C_p/T^3 versus T representation of our heat capacity data. Natural α -HgS sample: \circ ; artificial vapor phase grown sample: \blacklozenge . The solid line represents our theoretical data. Data by Khattak *et al.* [5] are represented by \square .

Measuring the heat capacity of isotope enriched samples can be favorably employed to test the *ab initio* calculations. Isotope enrichment of one of the constituents of α -HgS allows to selectively alter its mass and thus induce small variations in the phonon dispersion relations. In view of the clearly structured spectrum of the PDOS, isotope enrichment of Hg or S is expected to change the heat capacity in different temperature regimes. The small differences in the heat capacity of the isotope enriched samples with respect to the samples prepared from the elements with the natural isotope composition are barely seen in the C_p/T^3 -plot. We have demonstrated that the small changes can be clearly revealed in the logarithmic derivatives of C_p/T^3 versus the isotope masses (Fig. 4).

Two pronounced features are observed in the logarithmic derivative versus the mass of the S constituent (Fig. 4(a)), a rather pronounced sharp peak at ≈ 6 K and a broad hump with maximum at ≈ 100 K and probably a shoulder at ≈ 50 K. The broad feature reflects the two broad S-like bands in the PDOS between 150 cm^{-1} and 180 cm^{-1} and between 250 cm^{-1} and 350 cm^{-1} .

The origin of the sharp low-temperature peak at 10 K is not immediately obvious from the PDOS. We attribute it to a small mixture of Hg- and S-like phonons which also explains the small spike in the S-like phonon partial DOS at about 50 cm^{-1} . All features, especially the broad hump peaking at ≈ 100 K, are fairly well-reproduced in position and magnitude by the results of our calculations (Fig. 4).

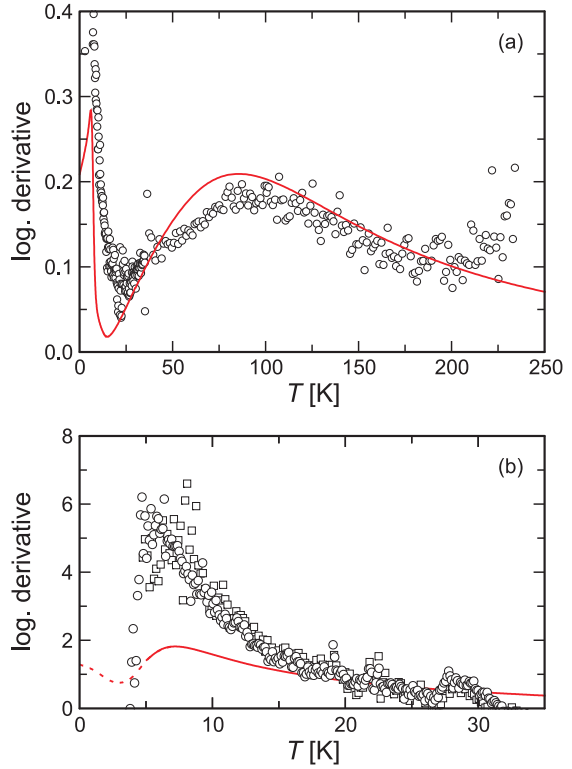


Figure 4: Logarithmic derivatives with respect to the masses m of the constituents Hg or S, $d \ln(C_p/T^3)/d \ln m$, of the experimental heat capacities. (a) Compares α - $^{\text{nat}}\text{Hg}^{\text{nat}}\text{S}$ with a sample of α - $^{\text{nat}}\text{Hg}^{34}\text{S}$. (b) Logarithmic derivative calculated by comparing samples of α - $^{\text{nat}}\text{Hg}^{\text{nat}}\text{S}$ and α - $^{198.9}\text{Hg}^{\text{nat}}\text{S}$. Different symbols (\circ , \square) indicate independent runs on samples of the same preparation. The (red) solid lines represent the logarithmic derivatives obtained from our theoretical data calculated for various isotope masses.

The agreement between experiment (two separate runs on two separately prepared samples from the same batch of isotopically enriched Hg) and theory for the logarithmic derivative w.r.t. the mass of the Hg atoms. A peak occurs in the logarithmic derivative at ≈ 6 K which corresponds well with the position expected from theory. But the experimental peak overshoots the theoretical calculation by almost a factor of three. The origin of this difference might be due to a small traces of metacinnabar β -HgS in our sample or other related effects. β -HgS has a significantly higher low-temperature heat capacity than α -HgS, in C_p/T^3 representation the peak is by a factor of three higher than that of α -HgS [2]. Comparing the heat capacities of the two modifications of HgS we estimate that a 1.5% admixture of β -HgS into our sample, probably hardly noticeable by visual inspection, would

be sufficient to explain the increase of the magnitude of the 6 K peak in the logarithmic derivative versus the Hg mass of α -HgS. The high cost of mercury isotopes has prevented a more detailed analysis of this anomaly.

In summary, we present a discussion of the lattice dynamical properties of cinnabar, α -HgS. We compare up-to-date *ab initio* calculations of the phonon dispersion with experimental results and find good agreement of experiment and theory.

References:

- [1] *Plinius Secundus, C.* Natural History, translated by H. Rackham; Book XXXIII, Vol. **IX**, 123, p. 93; Harvard University Press, Cambridge, MA (1961).

- [2] For more details of the *ab initio* calculations please c.f.: *Cardona, M., R.K. Kremer, R. Lauck, G. Siegle, A. Muñoz and A.H. Romero.* Physical Review B **80**, 195204 (2009); *Cardona, M., R.K. Kremer, G. Siegle, A. Muñoz, A.H. Romero and M. Schmidt.* Physical Review B **82**, 085210 (2010).
- [3] *Zallen, R., G. Lucovsky, W. Taylor, A. Pinczuk and E. Burstein.* Physical Review B **1**, 4058–4070 (1970); *Nusimovici, M.A. and G. Gorre.* Physical Review B **8**, 1648–1656 (1973).
- [4] *Schäfer, H.* Chemische Transportreaktionen; Verlag Chemie, Weinheim (1962).
- [5] *Khattak, G.D., H. Akbarzadeh and P.H. Keesom.* Physical Review B **23**, 2911–2915 (1981).

¹ Universidad de La Laguna, Tenerife, Spain

² Unidad Querétaro, Mexico

³ Max-Planck-Institut für Chemische Physik fester Stoffe, Dresden